SCIENTIFIC REPORTS

OPEN

Received: 17 April 2015
Accepted: 24 August 2015
Published: 23 September 2015

Parameterization of clear-sky surface irradiance and its implications for estimation of aerosol direct radiative effect and aerosol optical depth

Xiangao Xia

Aerosols impact clear-sky surface irradiance ($E_{g\downarrow}$) through the effects of scattering and absorption. Linear or nonlinear relationships between aerosol optical depth (τ_a) and $E_{g\downarrow}$ have been established to describe the aerosol direct radiative effect on $E_{g\downarrow}$ (ADRE). However, considerable uncertainties remain associated with ADRE due to the incorrect estimation of $E^0_{g\downarrow}$ (τ_a in the absence of aerosols). Based on data from the Aerosol Robotic Network, the effects of τ_a, water vapor content (w) and the cosine of the solar zenith angle (μ) on $E_{g\downarrow}$ are thoroughly considered, leading to an effective parameterization of $E_{g\downarrow}$ as a nonlinear function of these three quantities. The parameterization is proven able to estimate $E^0_{g\downarrow}$ with a mean bias error of 0.32 W m^{-2}, which is one order of magnitude smaller than that derived using earlier linear or nonlinear functions. Applications of this new parameterization to estimate τ_a from $E_{g\downarrow}$, or vice versa, show that the root-mean-square errors were 0.08 and 10.0 Wm^{-2}, respectively. Therefore, this study establishes a straightforward method to derive $E_{g\downarrow}$ from τ_a or estimate τ_a from $E_{g\downarrow}$ measurements if water vapor measurements are available.

Surface irradiance, the downwelling solar radiation from the Sun and sky that reaches the surface ($E_{g\downarrow}$), is the ultimate energy source for the Earth's climate system and life on the planet. A large number of diverse surface processes are governed by the amount of $E_{g\downarrow}$; for example, evaporation, snow/glacier melt and plant photosynthesis. Therefore, $E_{g\downarrow}$ plays an important role in studies of hydrological and carbon cycling[1–3]. Aerosols scatter and absorb solar radiation and thereby modulate the amount of clear-sky $E_{g\downarrow}$ ($E_{g\downarrow}$ hereafter). We define the aerosol direct radiative effect on $E_{g\downarrow}$ (ADRE) as the attenuation of clear-sky $E_{g\downarrow}$ due to aerosol scattering and absorption, i.e., the difference between $E_{g\downarrow}$ and $E^0_{g\downarrow}$ ($E_{g\downarrow}$ in the absence of aerosols). ADRE is widely reported in the literature, based on a combination of measurements of $E_{g\downarrow}$ and aerosol optical depth (τ_a)[4–7]. $E^0_{g\downarrow}$ cannot be obtained straightforwardly from observations since the atmosphere almost has aerosols present. One of the difficulties relating to the derivation of ADRE stems from the need to accurately estimate $E^0_{g\downarrow}$[7,8]. Radiative transfer model or single-layer clear-sky solar radiation model can be used to calculate $E^0_{g\downarrow}$[9–12] and thereby ADRE is obtained, however, this method is sensitive to the calibration uncertainties of pyranometer (independent of model calculation) and dependent on model assumptions about the atmospheric parameters[13]. $E^0_{g\downarrow}$ can be estimated from observations, this method avoids dependence on a model, furthermore, ADRE estimation should not be very sensitive to the calibration errors since $E^0_{g\downarrow}$ is derived from observations[13]. A linear relationship of $E_{g\downarrow}$ to τ_a has been popularly assumed and $E^0_{g\downarrow}$ is then derived by linear regression

LAGEO, Institute of Atmospheric Physics, Chinese Academy of Sciences, Beijing, China. Correspondence and requests for materials should be addressed to X.X. (email: xxa@mail.iap.ac.cn)

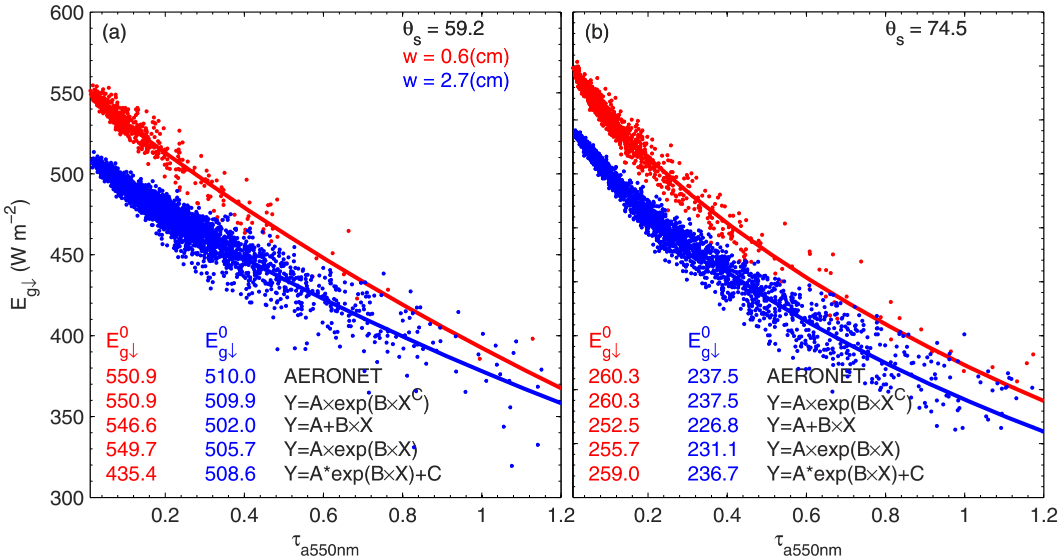

Figure 1. Scatter-plot of aerosol optical depth (τ_a) and surface irradiance ($E_{g\downarrow}$) for a solar zenith angle of (a) 59.2° and (b) 74.5°, and water vapor of 0.6 cm (red) and 2.7 cm (blue). These x-marks represent the Aerosol Robotic Network model calculation of surface irradiance in the absence of aerosols ($E^0_{g\downarrow}$). The values given in the first line represent the mean $E^0_{g\downarrow}$ by the Aerosol Robotic Network model calculation, and the following values are $E^0_{g\downarrow}$ derived on the basis of Eqs (1)–(4). The figure was produced using MATLAB.

analysis of $E_{g\downarrow}$ and τ_a[4,5,13]. Some studies suggested that an exponential decay of $E_{g\downarrow}$ with an increase in τ_a would be expected according to Beer–Lambert Law, which is especially true for cases with τ_a values larger than 0.5[7,8,13]. However, contrary to expectation, a better estimation of $E^0_{g\downarrow}$ was derived from the linear regression than using the exponential relationship. This was thought to be because the systematic underestimation of $E^0_{g\downarrow}$ by the linear regression was compensated by the positive correlation between τ_a and water vapor content (w)[8].

In this study, we show that these previous methods produce a systematic bias in the derivation of $E^0_{g\downarrow}$ and thereby result in an overestimation of ADRE. A new parameterization of $E_{g\downarrow}$ is developed based on global Aerosol Robotic Network (AERONET) data, in which the relationships of $E_{g\downarrow}$ to the cosine of the solar zenith angle (μ), τ_a and w have been established by using a combination of nonlinear equations. The results show that the mean bias error (MBE) of the estimations of $E^0_{g\downarrow}$ decreases from 4–7 W m^{-2} to 0.32 W m^{-2}. The same improvement in the estimation of ADRE would be expected when using the new method. Furthermore, one of the important advantages of this parameterization is that a straightforward method to derive τ_a from $E_{g\downarrow}$, or vice versa, has been established. Specifically, we find it is possible to derive τ_a from $E_{g\downarrow}$ with a root-mean-square error (RMSE) of 0.08, and vice versa with an RMSE of 10.0 W m^{-2}.

Results

The solid dots in Fig. 1 represent the scatter between τ_a at 550 nm (τ_a hereafter) and $E_{g\downarrow}$ at two narrow μ and w ranges. The analysis is firstly performed on data points with a very narrow range of μ (~0.2°) and w (10%w), to isolate the effect of τ_a on $E_{g\downarrow}$. The mean $E^0_{g\downarrow}$ amounts, using the AERONET calculation and fitting $E^0_{g\downarrow}$ values using regression analysis on the basis of Eqs (1)–(4) in the Method section, are also presented. The performance of these equations is evaluated by the agreement in instantaneous $E^0_{g\downarrow}$ between the AERONET calculations and the regression analysis results. We can see that the best performance is achieved using Eq. (4), the new parameterization proposed in this study, which produces a difference in $E^0_{g\downarrow}$ between the mean AERONET calculation and the regression analysis result ($\Delta E^0_{g\downarrow}$) of nearly zero. This nearly zero $\Delta E^0_{g\downarrow}$ is in fact always derived using Eq. (4) for the full μ and w ranges (not shown). In contrast, $\Delta E^0_{g\downarrow}$, when using Eqs (1), (2) and (3), varies from a few to tens of W m^{-2} in these two cases. The fact that Eq. (3) occasionally produces unrealistic results that indicate the poor performance of the nonlinear regression analysis[8], we eliminate it hereafter. Poorer performance of Eqs (1) and (2) than Eq. (4) is further shown by the histogram of $\Delta E^0_{g\downarrow}$ for Eqs (1) and (2) given in Fig. 2. Both equations nearly always underestimate $E^0_{g\downarrow}$. The mean bias error (MBE) and RMSE of $E^0_{g\downarrow}$ estimations are 6.8 (2.6) W m^{-2} for Eq. (1) and 3.6 (1.9) W m^{-2} for Eq. (2). The fact that Eq. (1) produces a considerably poorer result than Eq. (2) clearly shows the superiority of using nonlinear regression to

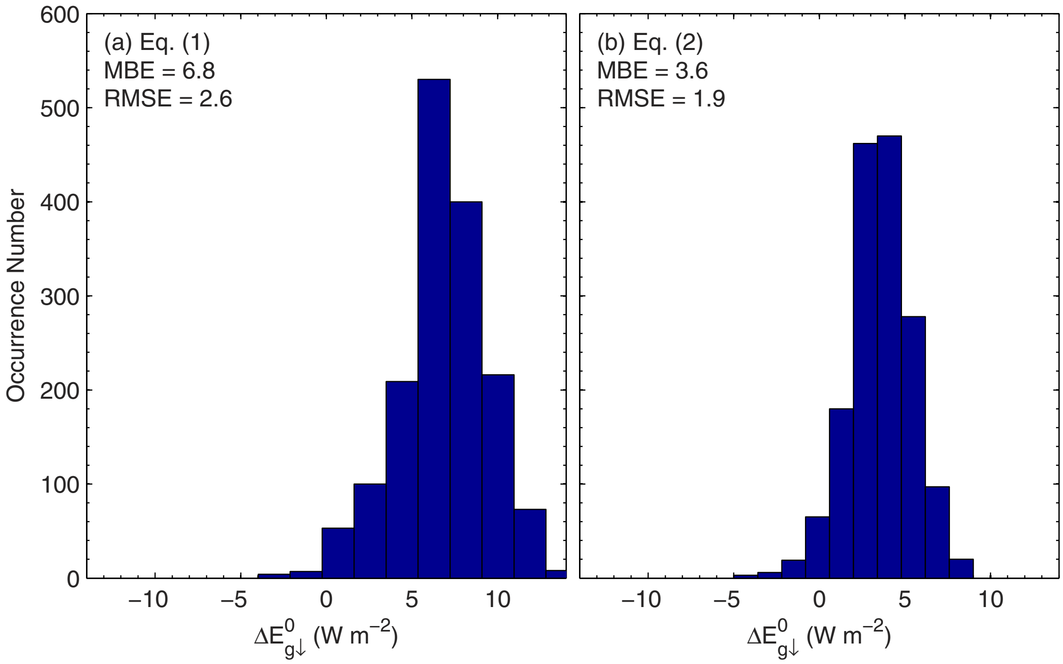

Figure 2. Histogram of the difference in surface irradiance in the absence of aerosols between the Aerosol Robotic Network model calculations and regression results using Eqs (1) and (2) ($\boldsymbol{\Delta E^0_{g\downarrow}}$). The given values are the mean bias and root-mean-square error of Eqs (1) and (2). The figure was produced using MATLAB.

extrapolate $E_{g\downarrow}$ to zero τ_a rather than linear regression. This conclusion is also supported by the fact that smaller residuals of the regression analysis are derived from Eq. (2) than from Eq. (1). This is expected because attenuation of $E_{g\downarrow}$ by aerosols shows nonlinear decay, as implied by Beer–Lambert Law.

The difference between Eq. (2) and Eq. (4) is the introduction of a new parameter, C, into Eq. (4). The value of C is nearly always lower than 1.0 (the exact value of Eq. (3)), which is one of the most important reasons for the better performance of Eq. (4). Eq. (3) is somewhat similar to Beer–Lambert Law, which depicts the attenuation of solar direct radiation by aerosols; however, some part of the attenuation of solar direct radiation is backscattered to the surface, which is certain to enhance $E_{g\downarrow}$. It is therefore expected that C should be lower than 1.0. In addition, the effect of aerosols on $E_{g\downarrow}$ should not be independent from μ, since μ governs the transfer path of photons. This implies that C should vary with μ, which is reflected in the following analysis.

Figure 3 presents the dependence of $E^0_{g\downarrow}$ (A in Eq. (4)), on w and μ. Variation of $E^0_{g\downarrow}$ is mainly governed by μ, which is somewhat modulated by w at the same value of μ. Therefore, parameter A for a given amount of w is firstly simulated using a power law function of μ (Eq. (5) in the Methods section). The first and most important reason for the selection of a power law function is because it models the simple physics of the situation with only two parameters[14,15]. Parameter a_1 of Eq. (5) represents expected measurements of $E^0_{g\downarrow}$ for a μ of 1. Parameter a_2 governs the $E^0_{g\downarrow}$ variation with μ. The second reason for selection of a power law function is that it provides a faithful approximation to the data.

Since the dependence of $E^0_{g\downarrow}$ on μ is depicted by parameters a_1 and a_2 of Eq. (5), the w effect on $E^0_{g\downarrow}$ is further simulated through the parameterization of a_1 and a_2 as a function of w. Figure 4 shows the relationships of a_1 and a_2 to w. We can see that the effect of water vapor per one unit of w on $E^0_{g\downarrow}$ decreases as w increases, which is expected since the relative increase in water vapor absorption gradually decreases as w increases[16]. These relationships are simulated using an exponential equation. The RMSEs of the regression analysis for a_1 and a_2 of Eq. (5) are 1.37 and 0.0004, respectively, indicating a faithful approximation. A parameterization of $E^0_{g\downarrow}$ to μ and w can then be established through a combination of Eqs (5)–(7) that leads to Eq. (8). Therefore, it is straightforward to calculate $E^0_{g\downarrow}$ from Eq. (8) if w is available, since μ can be calculated from location and time very accurately.

Further analysis of parameters B and C of Eq. (4) shows that both parameters are moderately related to μ and w, which thereby leads to a parameterization of $E_{g\downarrow}$ as a function of τ_a, μ and w. As shown in Fig. 5, parameters B and C are approximated well using Eqs (9) and (10). In terms of the variability of both parameters, 99.8% is explained by the regression analysis. Since the relationship between instantaneous $E_{g\downarrow}$ to τ_a as well as w for a specified value of μ is established, therefore, a straightforward method is developed that can be used to derive $E_{g\downarrow}$ if τ_a and w are available from another source, such as satellite

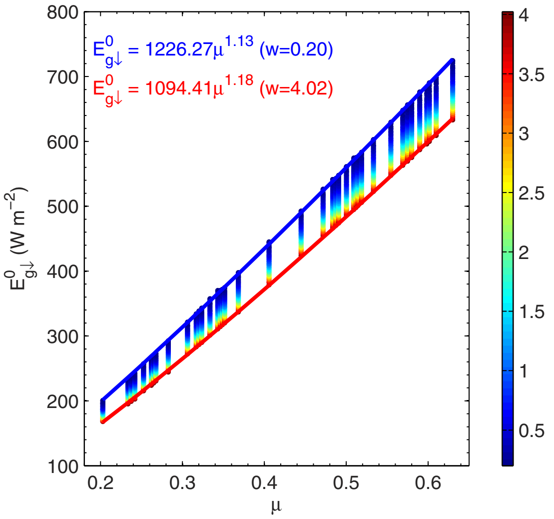

Figure 3. Scatter-plot of the cosine of the solar zenith angle (μ) and surface irradiance in the absence of aerosols ($E^0_{g\downarrow}$). The color bar represents the water vapor content (cm). The curve represents the regression result for a specified water vapor content of 0.20 cm (blue) and 4.02 (red). The figure was produced using MATLAB.

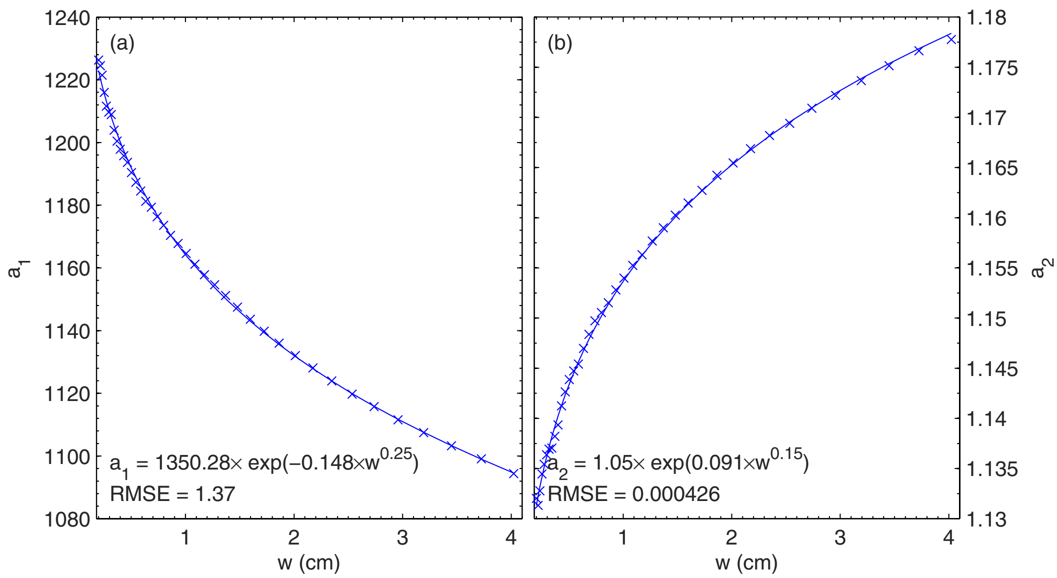

Figure 4. Scatter-plot of water vapor content and parameters (a) a_1 and (b) a_2 ofEq. 5. The curve represents the regression result using Eqs (6) and (7). The figure was produced using MATLAB.

remote sensing. On the other hand, it can also be used to derive τ_a if $E_{g\downarrow}$ and w are available from sources such as the Baseline Surface Radiation Network (BSRN). The proposed method is evaluated by using the 20% of validating data and BSRN data at Xianghe.

Figure 6a shows the comparison of instantaneous AERONET $E^0_{g\downarrow}$ values of validating data and calculations from Eq. (8) based on validating AERONET τ_a and w. The MBE is 0.33 W m^{-2}, one order magnitude smaller than the results from Eq. (1) and (2), even though the latter is derived from the training data. Since $E^0_{g\downarrow}$ is simulated well by Eq. (5), the ADRE derivation based on Eq. (5) should be very close to that derived from the AERONET model calculations. This expectation is supported by Fig. 6b, in which the AERONET ADREs are compared with estimations from Eq. (8). The MBE and RMSE values are −0.32 and 2.52 W m^{-2}, respectively.

To test the effectiveness of the parameterization of $E_{g\downarrow}$, the instantaneous AERONET τ_a and w values from the testing data points are substituted into Eqs (8)–(10) to estimate $E_{g\downarrow}$ values that are then compared with the AERONET $E_{g\downarrow}$ products. Similarly, τ_a values are estimated from AERONET $E_{g\downarrow}$ and w

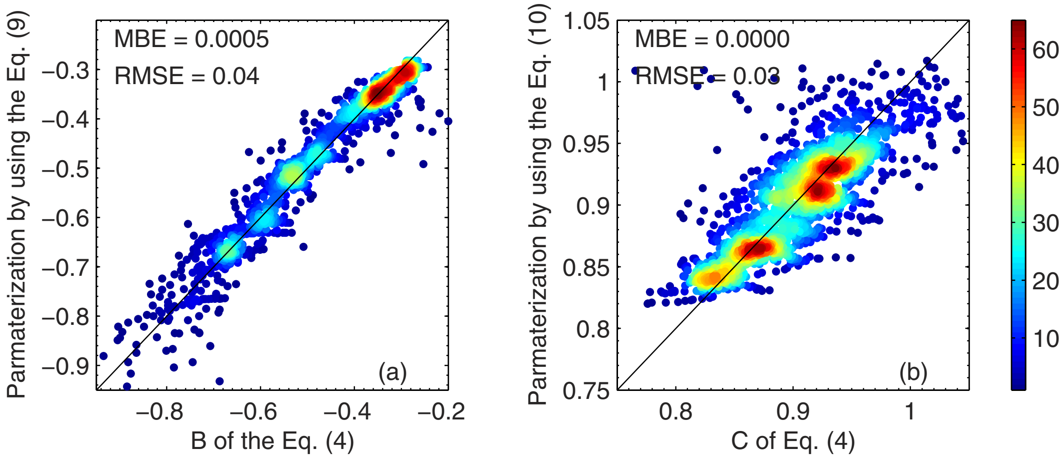

Figure 5. Density plot of parameters (a) *B* and (b) *C* of Eq. 4 and their parameterization results using Eqs (9) and (10). The color scale represents the relative density of points, where orange to red colors (levels ~45–60) indicate the highest number density. The mean bias error and root-mean-square error of the parameterization are also included. The figure was produced using MATLAB.

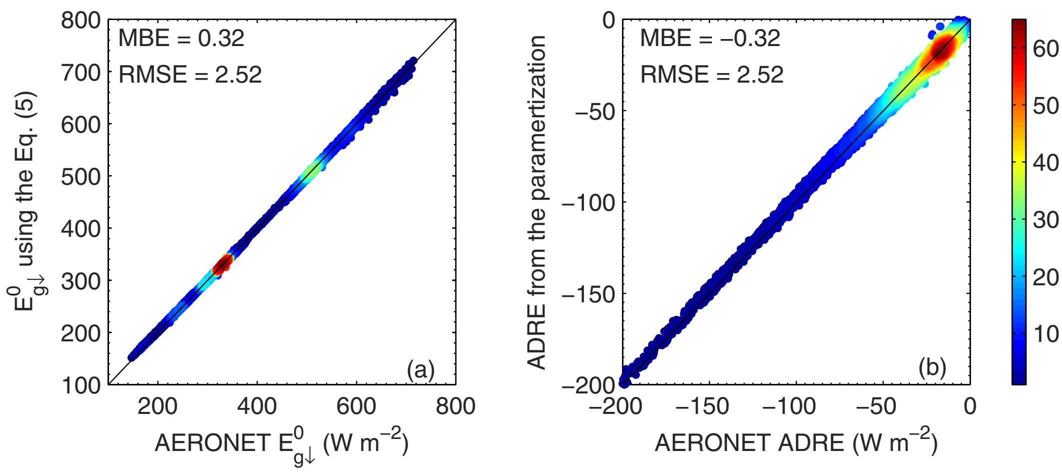

Figure 6. Density plot of AERONET (a) $E^0_{g\downarrow}$ and (b) ADRE and their parameterization results using Eqs (8). The color scale represents the relative density of points, where orange to red colors (levels ~ 45–60) indicate the highest number density. The mean bias error and root-mean-square error of the parameterization are also included. The figure was produced using MATLAB.

values and compared with AERONET τ_a products. Figure 7a shows that $E_{g\downarrow}$ can be estimated with an MBE and RMSE of 0.02 and 10.0 W m^{-2}, respectively. This certainly relies on the fact that both τ_a and w are available. On the contrary, if w and $E_{g\downarrow}$ are available and τ_a is not known, τ_a can be retrieved from $E_{g\downarrow}$ and w using this parameterization. The MBE and RMSE values of τ_a retrievals are 0.0005 and 0.08, respectively (Fig. 7b).

Measurements of $E_{g\downarrow}$ and τ_a at Xianghe[7], a BSRN and AERONET station in China are used to further evaluate the effectiveness of the parameterization of $E_{g\downarrow}$. The results are shown in Fig. 8. The estimations of $E_{g\downarrow}$ from AERONET τ_a and w products using the proposed parameterization method agree with the BSRN measurements very well, with an MBE and RMSE of -3.9 and 12.5 W m^{-2}, respectively. On the other hand, the retrievals of τ_a from the measurements of $E_{g\downarrow}$ and w are compared with AERONET τ_a products and the MBE and RMSE values are -0.03 and 0.08, respectively. These results once again proved the reliability of the proposed parameterization method.

Uncertainty analysis. In the parameterization of $E^0_{g\downarrow}$ (Eq. 8 of the Method section), surface albedo effect was excluded that likely produced bias in the estimation of $E^0_{g\downarrow}$. Figure 9 shows the scatter-plot of

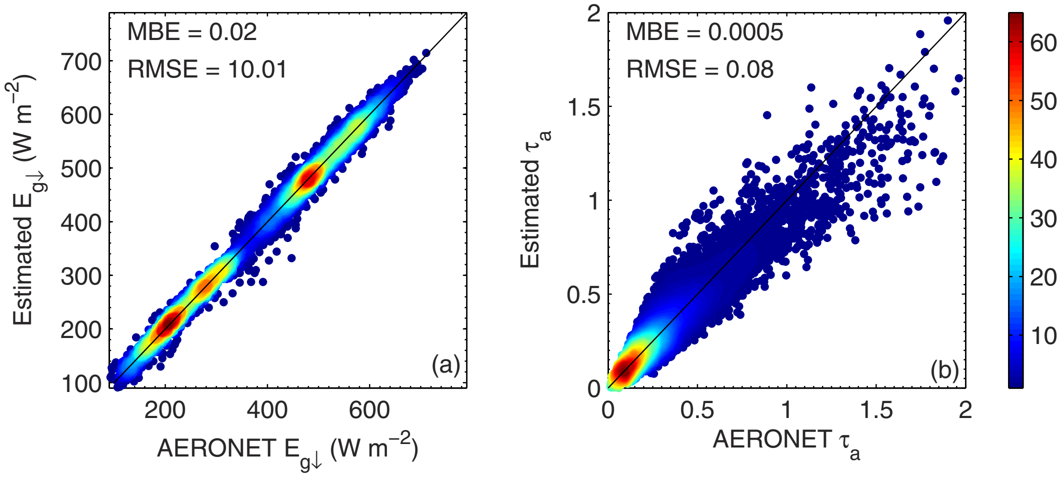

Figure 7. Density plot of AERONET (a) $E_{g\downarrow}$ and (b) τ_a and their parameterization results using Eqs (8–10). The color scale represents the relative density of points, where orange to red colors (levels ~ 45–60) indicate the highest number density. The mean bias error and root-mean-square error of the parameterization are also included. The figure was produced using MATLAB.

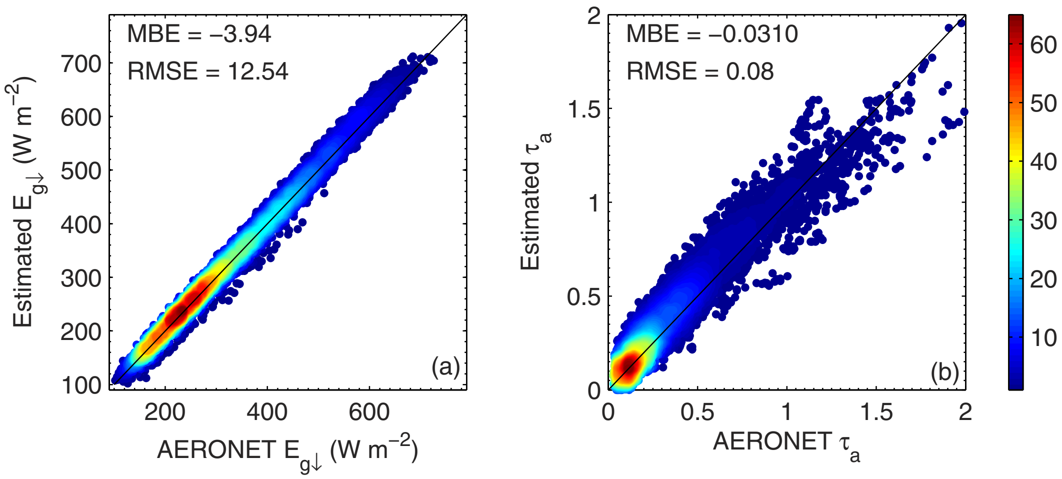

Figure 8. Similar as Fig. 7 but for the results from AERONET and BSRN data at Xianghe. The figure was produced using MATLAB.

surface albedo and $\Delta E^0_{g\downarrow}$, from which we can see a significant negative correlation between both quantities. Uncertainty of 0.1 in surface albedo may produce 1–3 W m^{-2} bias in $E^0_{g\downarrow}$.

τ_a is the dominant aerosol optical property driving the variation of $E_{g\downarrow}$ and therefore ADRE. However, aerosol absorption also plays an important role in ADRE[17], which shows a wide range of variations and thereby may lead to uncertainties in the parameterization of $E_{g\downarrow}$, since it was not accounted for. Remarkable impact of aerosol single scattering albedo at 550 nm (ω_{550nm}) on the estimation of $E_{g\downarrow}$ is presented in Fig. 10. $E_{g\downarrow}$ changes as a result of uncertainty of ω_{550nm} (0.03) was estimated to be a few Wm^{-2} that depends on optical path and τ_a. Significant impacts of ω_{550nm} on estimation of $E_{g\downarrow}$ from τ_a are further evidenced in Fig. 11 in which $\Delta E^0_{g\downarrow}$ shows a significant correlation to ω_{550nm}. The best estimation is achieved for ω_{550nm} of ~0.90 that is close to the median value of ω_{550nm} of AERONET data points.

In the above error analysis of $E^0_{g\downarrow}$, water vapor is assumed to be known without any uncertainty. This is, of course, not realistic, since water vapor products from AERONET, satellite measurements are not free of uncertainty. By differentiating Eq. (8) with respect to w, the uncertainty of $E^0_{g\downarrow}$ is estimated to be <3 W m^{-2} that is slightly dependent on optical path if the uncertainty of w is assumed to be $<10\%$ of w. The uncertainty of $E_{g\downarrow}$ estimation was estimated to <2 W m^{-2} if AERONET τ_a products with uncer-

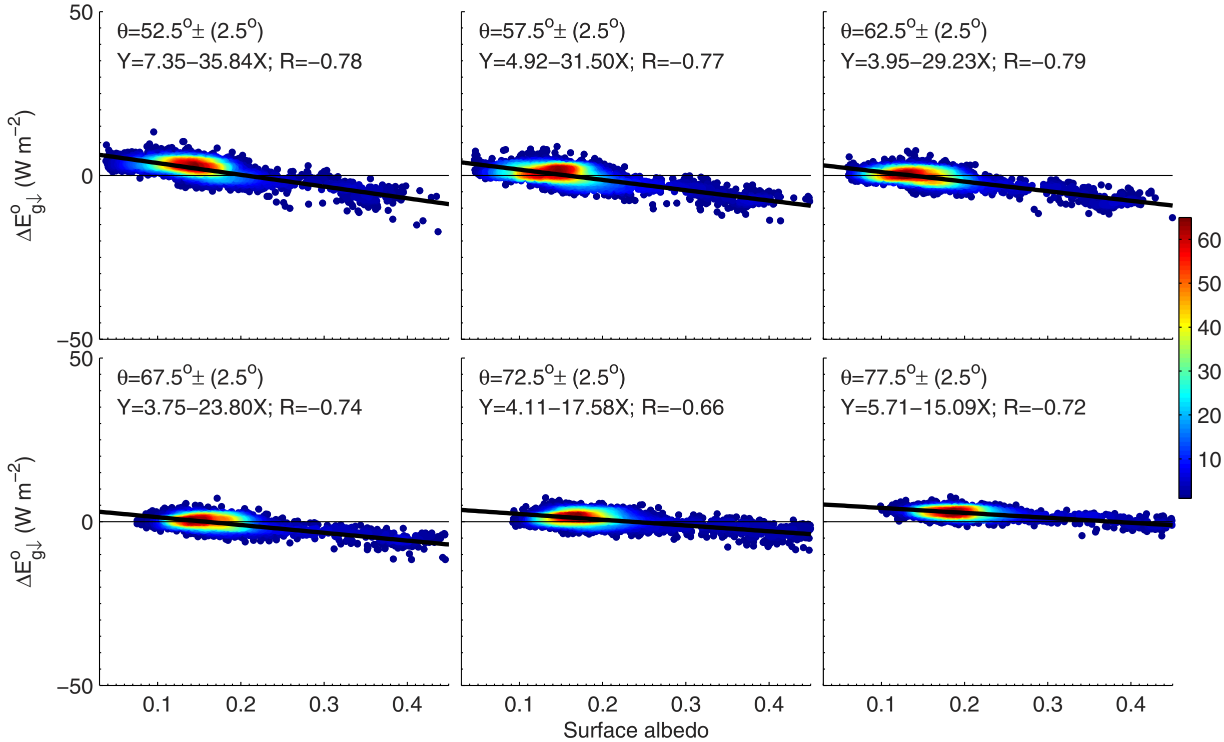

Figure 9. Scatter-plot of shortwave surface albedo to the difference in $E^0_{g\downarrow}$ between AERONET product and estimation using the proposed method for six solar zenith angle ranges. The figure was produced using MATLAB.

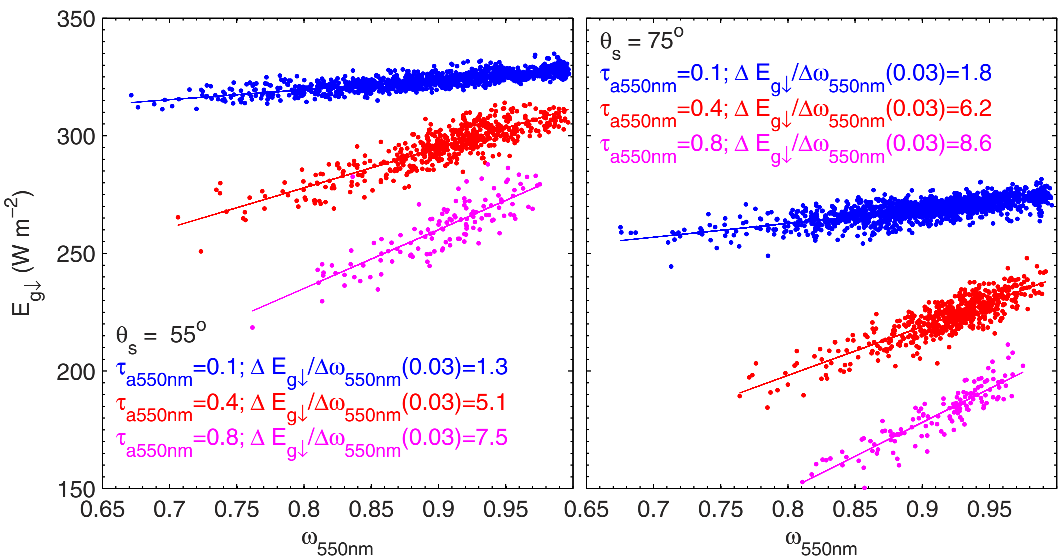

Figure 10. Scatter-plot of ω_{550nm} to $E_{g\downarrow}$ for three τ_a values and two solar zenith angles. The figure was produced using MATLAB.

tainty of 0.01 ~ 0.02 are used. However, this may reach 10 W m^{-2} if satellite τ_a products are used since their uncertainty was estimate to be 20% of τ_a over land[18]. The uncertainly of BSRN $E_{g\downarrow}$ measurements is estimate to be 2%[19], which may lead to the uncertainty of $\tau_a < 0.02$.

Discussion

$E_{g\downarrow}$ is one of the key parameters governing a large number of diverse surface processes, and therefore accurate measurement or estimation of $E_{g\downarrow}$ is significant[1–3]. Surface $E_{g\downarrow}$ networks are still limited in

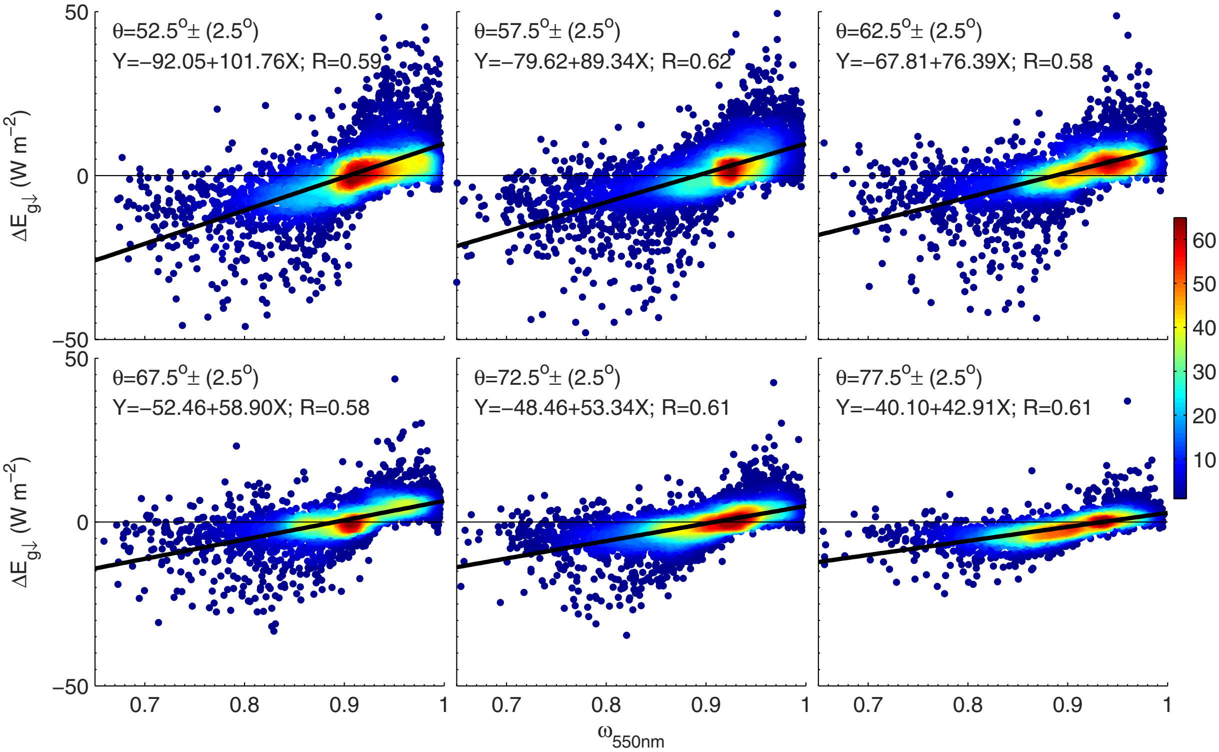

Figure 11. Scatter-plot of ω_{550nm} to the difference in $E^{0}_{g\downarrow}$ between AERONET product and estimation using the proposed method for six solar zenith angle ranges. The figure was produced using MATLAB.

spatial coverage; therefore, satellite remote sensing is a promising method for the accurate estimation of clear sky $E_{g\downarrow}$. Some highly complex algorithms have been developed to estimate $E_{g\downarrow}$ from satellite remote sensing data[20]. Given that τ_a values have been inverted from a few spaceborne radiometers since 2000 with good quality (e.g. the Moderate Resolution Imaging Spectraradiometer[18]), establishment of the parameterizations in this study provide a straightforward method to calculate clear sky $E_{g\downarrow}$ from such satellite aerosol products.

Broadband pyranometer measurements have been used to retrieve τ_a, which is e expected to be a promising method to build a long-term dataset of aerosol loading, since early pyranometer measurements can be tracked to the beginning of the last century[1]. Broadband direct solar radiation is widely used in these previous studies[21–23]. The method proposed in this study is based on global solar radiation measurements that are available more often than direct solar radiation. For example, there are only dozens of stations with direct solar radiation measurements; however, global solar radiation is measured at more than 100 stations in China. Certainly, it should be noted that measurement of global solar radiation is impacted by contamination of the upward facing glass dome, leveling of the instrument and cosine response of the pyranometer. The disadvantage of using direct solar radiation measurements is that it is occasionally disturbed by solar tracker malfunctions. Furthermore, both methods are impacted by calibration uncertainties.

The reason for only considering τ_a in the proposed method is that the availability of aerosol absorption is very limited, especially from satellite remote sensing. Similar analysis can be performed for a specified area characterized by a special aerosol type, e.g. dust aerosol in desert regions or biomass-burning aerosol in tropical forest regions. In this case, better performance of the parameterization is expected since aerosol absorption shows much less variation for the same aerosol type[24]. Furthermore, lower variation of surface albedo, ozone amount and surface elevation is also expected to reduce the random error of the parameterization.

Conclusion

Solar zenith angle, aerosol and water vapor are the three most important physical quantities governing the variability of $E_{g\downarrow}$. Based on a large quantity of AERONET τ_a, w, and $E_{g\downarrow}$ products, the effects of these quantities on $E_{g\downarrow}$ are fully considered, leading to an effective parameterization of $E_{g\downarrow}$ as a nonlinear function of these three quantities. The first advantage is that an accurate estimation of $E^{0}_{g\downarrow}$ is achieved, which ultimately results in a significant improvement of ADRE estimation compared to previous methods. The second is that a straightforward method has been established to estimate $E_{g\downarrow}$ from τ_a, or vice versa, if w is available. It is expected that potential applications of this new parameterization in the estimation of $E_{g\downarrow}$ and τ_a will arise in the near future.

Methods

I used $E_{g\downarrow}$, $E^0_{g\downarrow}$, τ_a and w products from those Aerosol Robotic Network (AERONET) sites with an elevation of less than 0.8 km (to eliminate the Rayleigh scattering effect on the analysis) (http://aeronet.gsfc.nasa.gov). The AERONET is a federation of ground-based remote sensing aerosol networks that is composed of more than 700 stations across the world (see Supplementary Fig. S1)[25]. The AERONET products were used because they cover different aerosol types ($0 < \tau_a < 3.0$; $0.65 < \omega_{550nm} < 1.0$; $-0.2 < \alpha_{440\_870nm} < 2.5$, see Supplementary Fig. S2) and thereby realistically represent the aerosol direct effect on $E_{g\downarrow}$. Furthermore, the availability of $E^0_{g\downarrow}$ data provides a benchmark for the evaluation of the parameterizations. Uncertainty of τ_a was estimated to be 0.01–0.02[26]. $E_{g\downarrow}$ and $E^0_{g\downarrow}$ were calculated using the discrete ordinates radiative transfer model with and without aerosols[27]. The $E_{g\downarrow}$ values agree with pyranometer measurements, with the relative difference varying from 0.98 to 1.02[28,29]. Of the 950,000 AERONET data points with surface albedo at 440 nm less than 0.25 (to reduce surface albedo effect on the analysis), I randomly select 80% of data points to develop the parameterization and the remaining 20% were used as test data. The analysis flow chart was presented in Supplementary (Fig. S3) that was described as follows.

To isolate the dependence of $E_{g\downarrow}$ on τ_a, the AERONET data were firstly divided into subgroups according to θ_s and w. The range of θ_s was 0.2°. The range of w was 10% of w (the measurement uncertainty[25]), respectively. The amount of $E_{g\downarrow}$ was normalized for the average Earth–Sun distance and cosine correction of $E_{g\downarrow}$ was performed within ranges to its midpoints. Three equations used in the literature were considered to represent the dependence of $E_{g\downarrow}$ on τ_a:

$$E_{g\downarrow} = A + B \times \tau_a \tag{1}$$

$$E_{g\downarrow} = A \times \exp(B \times \tau_a) \tag{2}$$

$$E_{g\downarrow} = A \times \exp(B \times \tau_a) + C \tag{3}$$

These equations were compared with the following new equation proposed in this paper:

$$E_{g\downarrow} = A \times \exp(B \times \tau_a^C) \tag{4}$$

The performance of these methods was evaluated using the $E^0_{g\downarrow}$ difference between the mean AERONET model calculations and the regression analysis result ($\Delta E^0_{g\downarrow}$). Given that Eq. (3) occasionally produces unrealistic results, we eliminated it in the comparison.

To derive $E^0_{g\downarrow}$ for varying μ and w, $E^0_{g\downarrow}$ was further parameterized as follows:

$$A_{\theta_s} = a_1 \times \mu^{a_2} \tag{5}$$

where a_1 and a_2 was found to relate to w as follows:

$$a_1 = 1350.3 \times \exp(-0.148 \times w^{0.25}) \tag{6}$$

$$a_2 = 1.05 \times \exp(0.091 \times w^{0.15}) \tag{7}$$

Therefore, the parameterization of $E^0_{g\downarrow}$ was finally developed through a combination of Eqs (5), (6) and (7).

$$A = (1350.3 \times \exp(-0.148 \times w^{0.25})) \times \mu^{(1.05 \times \exp(0.091 \times w^{0.15}))} \tag{8}$$

It was found that parameters B and C of Eq. (4) show moderate variation with μ and w, which was then simulated by the following equations:

$$B = (-0.0024 \times w^{-2.105} - 0.188) \times \mu^{-0.879} \tag{9}$$

$$C = 1.295 \times \mu + 0.019 \times w^{-0.955} + 0.759 \tag{10}$$

The parameterization of $E_{g\downarrow}$ to μ, w and τ_a was finally established. This parameterization can be used to estimate $E_{g\downarrow}$ by using a combination of Eq. 4 and 8–10 if τ_a and w are available, and conversely, τ_a can be directly calculated from $E_{g\downarrow}$ and w. μ can be accurately calculated from location and time.

References

1. Wild, M. Global dimming and brightening: A review. *J. Geophys. Res.* **114,** D00D16, doi: 10.1029/2008JD011470 (2009).
2. Mercado, L. M. *et al.* Impact of changes in diffuse radiation on the global land carbon sink. *Nature* **458,** 1014–U1087, doi: 10.1038/nature07949 (2009).
3. Wang, K. C. & Dickinson, R. E. Contribution of solar radiation to decadal temperature variability over land. *Proc Natl Acad Sci USA* **110,** 14877–14882, doi: 10.1073/pnas.1311433110 (2013).
4. Satheesh, S. K. & Ramanathan, V. Large differences in tropical aerosol forcing at the top of the atmosphere and Earth's surface. *Nature* **405,** 60–63, doi: 10.1038/35011039 (2000).
5. Conant, W. C. *et al.* A model for the radiative forcing during ACE-Asia derived from CIRPAS Twin Otter and R/V Ronald H. Brown data and comparison with observations. *J. Geophys. Res.* **108,** 8661, doi: 10.1029/2002JD003260 (2003).
6. Dumka, U. C. *et al.* Surface changes in solar irradiance due to aerosols over central Himalayas. *Geophys. Res. Lett.* **33,** L20809, doi: 10.1029/2006GL027814 (2006).
7. Xia, X. A., Li, Z. Q., Chen, H. B. & Cribb, M. Estimation of aerosol effects on surface irradiance based on measurements and radiative transfer model simulations in northern China. *J. Geophys. Res.* **112,** D22S10, doi: 10.1029/2006JD008337 (2007).
8. Huttunen, J. *et al.* Effect of water vapor on the determination of aerosol direct radiative effect based on the AERONET fluxes. *Atmos. Chem. Phys.* **14,** 6103–6110 (2014).
9. Gueymard, C. Clear-sky irradiance predictions for solar resource mapping and large-scale applications: Improved validation methodology and detailed performance analysis of 18 broadband radiative models. *Sol. Energy* **86,** 2145–2169 (2012).
10. Badescu, V. *et al.* Computing global and diffuse solar hourly irradiation on clear sky. Review and testing of 54 models. *Renew. Sust. Energy Rev.* **16,** 1636–1656 (2012).
11. Reno, M. J., Hansen, C. W. & Stein, J. S. Global Horizontal Irradiance Clear Sky Models: Implementation and Analysis, Sandia Nationa Lboratories. *Tech Report SAND* 2012–2389 (2012).
12. Gueymard, C. A. & Ruiz-Arias, J. A. Validation of direct normal irradiance predictions under arid conditions: A review of radiative models and their turbidity-dependent performance. *Renew. Sust. Energy Rev.* **45,** 379–396 (2015).
13. Conant, W. An observational approach for determining aerosol surface radiative forcing: results from the first field phase of INDOEX. *J. Geophys. Res.* **105,** 15347–15360 (2000).
14. Allen, R. J., Norris, J. R. & Wild, M. Evaluation of multidecadal variability in CMIP5 surface solar radiation and inferred underestimation of aerosol direct effects over Europe, China, Japan and India. *J. Geophy. Res.* **118,** 6311–6336, doi: 10.1002/jgrd.50426 (2013).
15. Long, C. N. & Ackerman, T. P. Identification of clear skies from broadband pyranometer measurements and calculation of downwelling shortwave cloud effects. *J. Geophys. Res.* **105,** 15609–15626 (2000).
16. Iqbal, M. *An introduction to solar radiation*. Elsevier (2012).
17. Xia, X. A critical assessment of direct radiative effects of different aerosol types on surface global radiation and its components. *J. Quant. Spec. Rad. Tran.* 149, 72–80 (2014).
18. Levy, R. *et al.* Global evaluation of the Collection 5 MODIS dark-target aerosol products over land. *Atmos. Chem. Phys.* **10,** 10399–10420 (2010).
19. Ohmura, A. *et al.* Baseline surface radiation network (BSRN/WCRP): new precision radiometry for climate research. *Bull. Amer. Meteo. Soc.* **79,** 2115–2136 (1998).
20. Hinkelman, L. M., Stackhouse, P. W., Wielicki, B. A., Zhang, T. P. & Wilson, S. R. Surface insolation trends from satellite and ground measurements: comparisons and challenges. *J. Geophys. Res.* **114,** D00D20, doi: 10.1029/2008JD011004 (2009).
21. Qiu, J. Q. A method to determine atmospheric aerosol optical depth using total direct solar radiation. *J. Atmos. Sci.* **55,** 744–757 (1998).
22. Diermendjian, D. A survey of light-scattering techniques used in the remote monitoring of atmospheric aerosol. *Rev. Geophys. Space Phys*. **18,** 341–360 (1980).
23. Gueymard, C. & Garrison, J. Critical evaluation of precipitable water and atmospheric turbidity in Canada using measured hourly solar irradiance. *Sol. Energy* **62,** 291–307 (1998).
24. Eck, T. *et al.* Climatological aspects of the optical properties of fine/coarse mode aerosol mixtures. *J. Geophys. Res.* **115,** D19205, doi: 10.1029/2010JD014002 (2010).
25. Holben, B. N. *et al.* AERONET—a Federated Instrument Network and Data Archive for aerosol characterization. *Remote Sens. Environ.* **66,** 1–16 (1998).
26. Eck, T. F. *et al.* Wavelength dependence of the optical depth of biomass burning, urban, and desert dust aerosols. *J. Geophys. Res.* **104,** 31333–31349, doi: 10.1029/1999JD900923 (1999).
27. Dubovik, O. & King, M. D. A flexible inversion algorithm for retrieval of aerosol optical properties from Sun and sky radiance measurements. *J. Geophys. Res.* **105,** 20673–20696, doi: 10.1029/2000JD900282 (2000).
28. García, O. E. *et al.* Validation of AERONET estimates of atmospheric solar surface fluxes and aerosol radiative forcing by ground-based broadband measurements. *J. Geophys. Res.* **113,** D21207, doi: 10.1029/2008JD010211 (2008).
29. Li, Z., Lee, K., Wang, Y., Xin, J. & Hao, W. First observation—based estimates of cloud-free aerosol radiative forcing across China. *J. Geophys. Res.* **115,** D00K18, doi: 10.1029/2009JD013306 (2010).

Acknowledgments

This research was funded by the Strategic Priority Research Program of the Chinese Academy of Sciences (XDA05100301) and the National Natural Science Foundation of China (41175031). AERONET PIs for the establishment and maintenance of AERONET stations are greatly appreciated.

Author Contributions

"X.A. wrote the main manuscript text and reviewed the manuscript".

Additional Information

Supplementary information accompanies this paper at http://www.nature.com/srep

Competing financial interests: The author declares no competing financial interests.

How to cite this article: Xia, X. Parameterization of clear-sky surface irradiance and its implications for estimation of aerosol direct radiative effect and aerosol optical depth. *Sci. Rep.* **5**, 14376; doi: 10.1038/srep14376 (2015).